Title:
Storm surge, not wind, caused mangrove dieback in southwest Florida following Hurricane Irma

Authors: David Lagomasino[1,*], Temilola Fatoyinbo[2], Edward Castañeda-Moya[3], Bruce D. Cook[2], Paul Montesano[4,2,] Christopher Neigh[2], Lawrence A. Corp[4,2], Lesley Ott[2], Selena Chavez[5], Douglas C. Morton[2]

Affiliations:
[1]Department of Coastal Studies, East Carolina University, Wanchese, NC, USA.
[2]Biospheric Sciences Laboratory, NASA Goddard Space Flight Center, Greenbelt, MD, USA.
[3]Southeast Environmental Research Center, Institute of Environment, Florida International University, Miami, FL, USA.
[4]Science Systems and Applications, Inc., Lanham, MD, USA.
[5]Department of Earth and Environment, Florida International University, Miami, FL, USA.

*Correspondence to: lagomasinod19@ecu.edu

Abstract

Mangroves buffer inland ecosystems from hurricane winds and storm surge. However, their ability to withstand harsh cyclone conditions depends on plant traits and geomorphology. Using airborne lidar and satellite imagery collected before and after Hurricane Irma, we estimated that 62% of mangroves in southwest Florida suffered canopy damage, with largest impacts in tall forests (>10 m). Mangroves on well-drained sites (83%) flushed new leaves within one year after the storm. In poorly-drained sites, Irma triggered one of the largest mangrove diebacks ever recorded (10,760 ha), primarily affecting low elevation and interior mangrove areas dominated or co-dominated by *A. germinans* (73%). Our results show storm surge and ponding caused dieback, not wind. Identifying and monitoring vulnerable, low-lying coastal areas is essential to mitigate mangrove dieback from future storms.

Main Text

Worldwide, mangrove forests safeguard inland ecosystems from coastal storms (*1, 2*). In the US alone, mangroves prevent $11.3 billion in property damage and 14,200 km^2 of flooding each year, with the greatest flood protection benefits during cyclones (*2*). Moreover, coastlines with extensive mangrove forests buffer coastal economies and reduce the period of economic inactivity following a hurricane by up to four months compared to areas with minimal mangrove cover (*1, 3*). Projected changes in the frequency and intensity of tropical cyclones (*4, 5*) may create a positive feedback whereby more frequent mangrove damages from tropical cyclones compromise the buffering capacity of mangroves in future storms (*6*).

Damage to mangrove forests from tropical cyclones varies from temporary defoliation to widespread tree mortality (*6, 7*). Recovery from storm damage also varies as a function of storm strength and edaphic conditions. In some cases, storms deposit phosphorous-rich sediments that

stimulate mangrove growth (*8*). However, in other areas, initial damages are compounded by
45   delayed mortality that can constrain mangrove recovery for months or years following a storm
(*7, 9*). Identifying the locations and the mechanisms that trigger widespread collapse of
mangrove forests is therefore critical for understanding the vulnerability of coastal ecosystems
and developing plans to mitigate dieback events from future storms.

50   South Florida is home to the largest tract of continuous mangrove forests in the United States.
Human development has hemmed in these mangroves and drastically altered the coastal
hydrology, leaving these forests vulnerable to sea level rise, salt water intrusion, and ponding
(*10, 11*). These chronic stressors are compounded by strong and sustained winds, storm surge,
and prolonged flooding during hurricane events, pushing mangroves to the brink of collapse (*7,
55   9*). The risk of dieback triggered by hurricane damages is dependent on mangrove structure,
species composition, geomorphology, and elevation (*8, 9*), in addition to the specific
characteristics of each hurricane (*12*).

In September 2017, Hurricane Irma made landfall in south Florida with winds in excess of 52
60   mps (116 mph) and storm surge as high as 3 m (Fig. 1). Mangroves along the southwest coast
experienced the full strength of the storm. Powerful winds stripped leaves and branches from
mangroves and snapped and uprooted trees. Storm surge reshaped coastal topography through
sedimentation, erosion, and inundation of low-lying areas. Together, structural damages to
mangroves and the reorganization of coastal geomorphology threaten the long-term stability of
65   the ecosystem by altering drainage patterns and disrupting forest succession (*13*). Previous
studies have used satellite imagery to track the damage and recovery of mangroves from
hurricanes (*12, 14*), but few studies have assessed the three-dimensional (3D) changes in
mangrove structure (*15*) needed to understand the diversity of hurricane impacts on mangrove
forests and the limits to mangrove resilience.
70
Here, we combined airborne and satellite remote sensing data to estimate mangrove damage and
recovery in the year following Hurricane Irma. Airborne lidar data were acquired before (April
2017) and after (December 2017) the storm by NASA Goddard's Lidar, Hyperspectral, and
Thermal (G-LiHT) airborne imager (*16*) to estimate the 3D changes in vegetation structure at 1-
75   m spatial resolution across 130,000 ha of coastal wetlands in south Florida (figs. S1-5). We
combined G-LiHT data with time series of Landsat imagery to track the recovery of coastal
ecosystems across gradients of structural damage (figs. S6-9), exposure to maximum hurricane
winds, storm surge, community composition, and ground elevation (*17*). We combined estimates
of structural damage and recovery trajectories with maps of species composition and topographic
80   elevation to identify the role of wind and storm surge for changes in mangrove forests, including
evidence for long-term dieback. Together, these data provided an unprecedented look at the
spatial and temporal patterns of mangrove damage and recovery following a major hurricane.

Structural damages to mangrove forests from Hurricane Irma varied based on wind exposure and
85   canopy height (Fig. 1). Strong and sustained winds reduced average canopy height by 1.16 m
(S.D. ± 1.36) (Table 1, table S1). Forests over 10 m decreased by an average of 2 to 3 m,
regardless of hurricane wind speed, whereas shorter trees suffered smaller losses (<1.2 m).
Reductions in canopy height reflect the loss of canopy branches and snapped or uprooted whole
trees (fig. S3-5). Using coincident high-resolution imagery from airborne and satellite platforms

90   (*17*), we estimated a 15.3% (±10.6%) reduction in mangrove canopy volume, a measure strongly correlated with aboveground biomass (*18*). The largest losses of canopy height and volume were concentrated in the major estuaries, areas with the tallest forest canopies and regular freshwater and tidal flushing (Fig. 1D).

95   Hurricane Irma also led to widespread mangrove canopy defoliation, measured as a loss of fractional vegetation cover (FVC). Irma reduced the extent of closed-canopy mangrove forests by 86%. Importantly, areas of greatest FVC loss were not collocated with the largest reductions in canopy height, except where Irma made landfall (Fig. 1D & E). Losses in canopy cover were widespread across the storm-affected area, whereas canopy height losses were primarily confined
100   to areas with the tallest trees.

      Satellite data time series provide an indication of the early trajectory of forest recovery following hurricane damages (Fig. 2), even though full a recovery of canopy structure and forest biomass can take decades. The spatial patterns of forest recovery in Florida following Hurricane Irma
105   highlight strong spatial patterns based on pre-storm forest structure, position in the tidal frame, and species composition that confer resilience to hurricane disturbances (*13*, *19*). Of the three dominant mangrove species in Florida, *Avicennia germinans* and *Laguncularia racemosa* have the ability of resprouting through epicormic growth after branch or stem damage, whereas *Rhizophora mangle* does not, typically leading to higher rates of mortality from hurricanes (*13*).
110
      Hurricane Irma triggered one of the largest recorded mangrove dieback events. In the first 15 months after Irma, 10,760 ha of mangroves showed evidence of complete dieback, with little to no greening. Despite their higher salt tolerance and resprouting ability, *A. germinans* trees were disproportionately affected by the die-off, with an estimated 7,750 ha (73%) of the damaged
115   forests dominated or co-dominated by the species (Fig. 2A). Irma also had a strong selective pressure on the distribution of *A. germinans*; nearly 40% of the mangrove forests with *A. germinans* died compared to the less than 6% of the other species.

      Delayed or failed mangrove recovery was primarily confined to low elevation, endorheic basins,
120   and interior portions of large continuous patches of mangrove forests (Fig. 2B&C). These regions were vulnerable to dieback from saltwater ponding because of the limited tidal range and hydrologic isolation (fig. S5). Impounded flood waters cut off from the tidal prism can create multiple biochemical stressors, particularly increases in porewater sulfide and decreases in redox potential, which causes the rapid degradation of fine root material and soil substrate, ultimately
125   leading to peat collapse (*20*). Artificial barriers such as roads and levees can obstruct the flow of water, exacerbating permanent flooding conditions, leading to mangrove die off as seen along the road near the Flamingo ranger station (Fig. 1I, 2C, fig. S5B). Similarly, natural shoreline embankments near Gopher Key and Cape Sable, formed by sediment deposited during minor storms, can also restrict drainage, increasing the susceptibility of impounded water during
130   extreme hurricanes (Fig. 2C & 3A). These two regions accounted for nearly 75% of the total dieback, despite not being in the direct path of the storm.

      The legacy from Hurricane Irma on southwest Florida differs from previous catastrophic storms in the region based on extensive mangrove forest dieback (*13*, *21*). Hurricane Donna (1960) was
135   the last major storm (category 4) to strike the region on a similar track over the Florida Keys and

Florida Bay (*22*). The south-to-north storm trajectory exposes some of the most vulnerable, low-lying coastal endorheic landscapes to the strongest hurricane winds and wind-driven storm surge (*23*). High storm surge from Hurricane Irma overtopped the Buttonwood Ridge, a relatively high natural coastal barrier (*24*) and became trapped (Fig. 3). Our regional analysis highlights the
140   spatial heterogeneity of forest damages, recovery rates, and vulnerability to mangrove dieback. Despite widespread wind damage from Hurricane Irma, extensive mangrove die-off resulted from the retention of storm surge water in enclosed or semi-enclosed basins.

Sea level rise and the projected increase in the frequency and severity of hurricanes with climate
145   change (*25*) provide strong motivation to augment traditional hurricane rating systems with specific metrics that account for storm surge and coastal geomorphology. In addition, integrated coastal monitoring networks can enhance the efficacy of surge warnings and mitigate future mangrove dieback events to protect both human and natural systems. For example, establishing field research stations in vulnerable, low-lying areas can help identify key physical and
150   biological processes that may be underrepresented in more pristine field sites (*26*). Regular coastal lidar surveys can locate and monitor endorheic basins to help inform risk assessments and prioritize rehabilitation or removal of barriers needed to improve hydrologic connectivity. Efforts to restore freshwater flow will help create new tidal channels and reduce the stress of prolonged saltwater flooding from high tides and storms in vulnerable mangroves. These monitoring and
155   mitigation efforts to enhance coastal resilience to future storms will require cooperation across multiple water resource agencies to reduce vulnerability in coastal communities and minimize economic losses during extreme events (*1–3*).
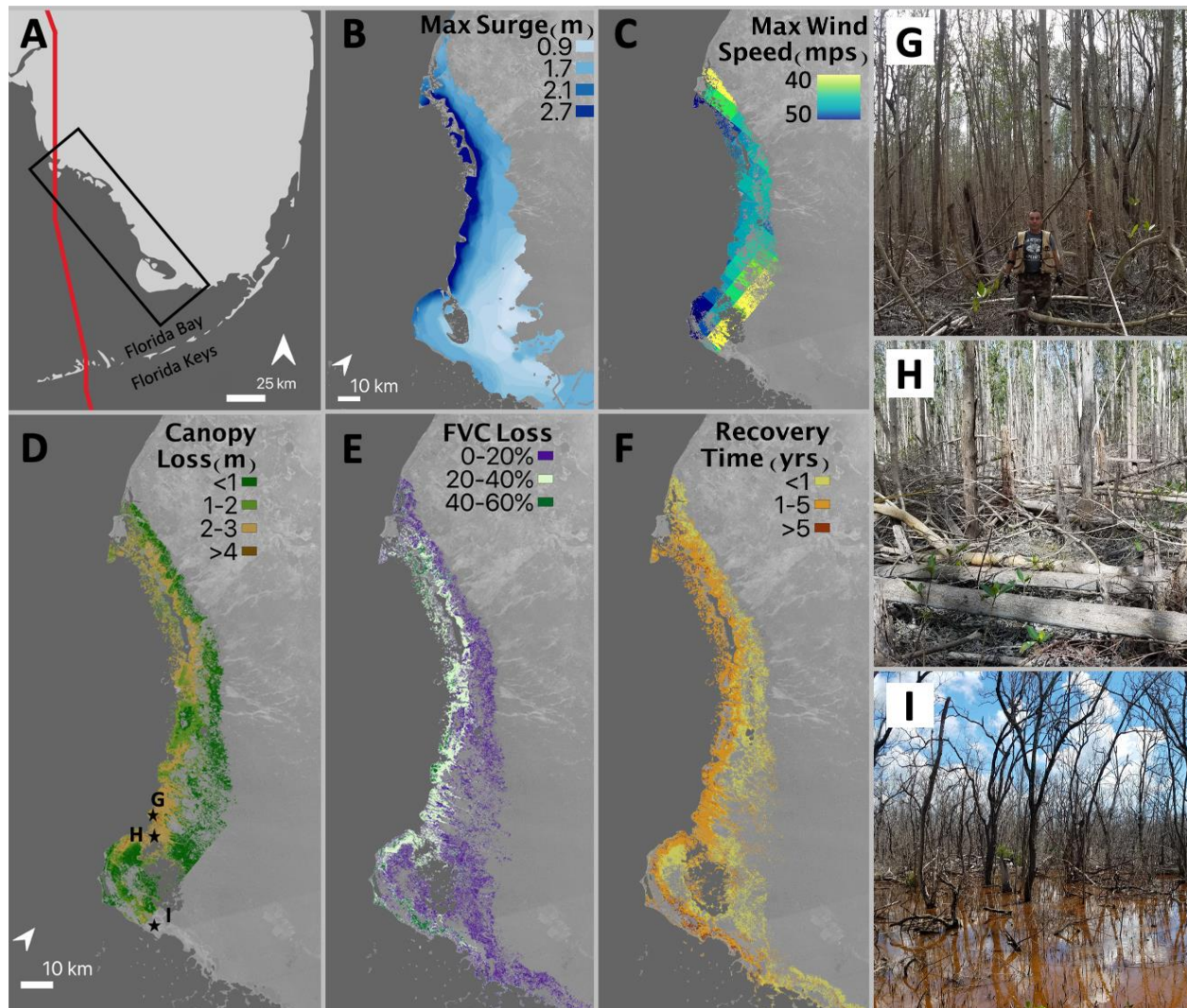
References

160   1.   J. P. Hochard, S. Hamilton, E. B. Barbier, Mangroves shelter coastal economic activity from cyclones. *Proc. Natl. Acad. Sci. U. S. A.* **116**, 12232–12237 (2019).

2.   P. Menéndez, I. J. Losada, S. Torres-Ortega, S. Narayan, M. W. Beck, The Global Flood Protection Benefits of Mangroves. *Sci. Rep.* **10**, 4404 (2020).

3.   A. del Valle, M. Eriksson, O. A. Ishizawa, J. J. Miranda, Mangroves protect coastal
165   economic activity from hurricanes. *Proc. Natl. Acad. Sci. U. S. A.* **117**, 265–270 (2020).

4.   K. Bhatia *et al.*, Projected Response of Tropical Cyclone Intensity and Intensification in a Global Climate Model. *J. Clim.* **31**, 8281–8303 (2018).

5.   A. H. Sobel *et al.*, Human influence on tropical cyclone intensity. *Science*. **353**, 242–6 (2016).

170   6.   T. M. Danielson *et al.*, Assessment of Everglades mangrove forest resilience: Implications for above-ground net primary productivity and carbon dynamics. *For. Ecol. Manage.* **404**, 115–125 (2017).

7.   D. R. Cahoon *et al.*, Mass tree mortality leads to mangrove peat collapse at Bay Islands, Honduras after Hurricane Mitch. *J. Ecol.* **91**, 1093–1105 (2003).

175   8.   E. Castañeda-Moya *et al.*, Hurricanes fertilize mangrove forests in the Gulf of Mexico (Florida Everglades, USA). *Proc. Natl. Acad. Sci. U. S. A.* **117**, 4831–4841 (2020).

9.   K. R. Radabaugh *et al.*, Mangrove Damage, Delayed Mortality, and Early Recovery Following Hurricane Irma at Two Landfall Sites in Southwest Florida, USA. *Estuaries and Coasts*, 1–15 (2019).

180   10.   S. Wdowinski, R. Bray, B. P. Kirtman, Z. Wu, Increasing flooding hazard in coastal communities due to rising sea level: Case study of Miami Beach, Florida. *Ocean Coast.*

Manag. **126**, 1–8 (2016).

11. J. F. Meeder, R. W. Parkinson, SE Saline Everglades Transgressive Sedimentation in Response to Historic Acceleration in Sea-Level Rise: A Viable Marker for the Base of the Anthropocene? *J. Coast. Res.*, 490–497 (2017).

12. X. Han, L. Feng, C. Hu, P. Kramer, Hurricane-Induced Changes in the Everglades National Park Mangrove Forest: Landsat Observations Between 1985 and 2017. *J. Geophys. Res. Biogeosciences.* **123**, 3470–3488 (2018).

13. T. J. Smith *et al.*, Cumulative impacts of hurricanes on Florida mangrove ecosystems: sediment deposition, storm surges and vegetation. *Wetlands.* **29**, 24–34 (2009).

14. C. Zhang, S. D. Durgan, D. Lagomasino, Modeling risk of mangroves to tropical cyclones: A case study of Hurricane Irma. *Estuar. Coast. Shelf Sci.* **224**, 108–116 (2019).

15. K. Zhang, Identification of gaps in mangrove forests with airborne LIDAR. *Remote Sens. Environ.* **112**, 2309–2325 (2008).

16. B. D. Cook *et al.*, NASA Goddard's LiDAR, Hyperspectral and Thermal (G-LiHT) Airborne Imager. *Remote Sens.* **5**, 4045–4066 (2013).

17. Materials and methods are available as supplementary materials.

18. T. Fatoyinbo, E. A. Feliciano, D. Lagomasino, S. Lee, C. Trettin, Estimating mangrove aboveground biomass from airborne LiDAR data: a case study from the Zambezi River delta. *Environ. Res. Lett.* **13**, 25012 (2018).

19. D. Imbert, Hurricane disturbance and forest dynamics in east Caribbean mangroves. *Ecosphere.* **9**, e02231 (2018).

20. A. Pérez, D. Gutiérrez, M. S. Saldarriaga, C. J. Sanders, Tidally driven sulfidic conditions in Peruvian mangrove sediments. *Geo-Marine Lett.* **38**, 457–465 (2018).

21. T. W. Doyle, T. J. Smith, M. B. Robblee, Wind Damage Effects of Hurricane Andrew on Mangrove Communities Along the Southwest Coast of. *J. Coast. Res.* **S1**, 159–168 (1992).

22. F. C. Craighead, V. C. Gilbert, The effects of Hurricane Donna on the vegetation of southern Florida. *Q. J. Florida Acad. Sci.* **25**, 1–28 (1962).

23. G. L. Wingard *et al.*, Impacts of Hurricane Irma on Florida Bay Islands, Everglades National Park, USA. *Estuaries and Coasts*, 1–20 (2019).

24. M. A. Sutula *et al.*, Factors affecting spatial and temporal variability in material exchange between the Southern Everglades wetlands and Florida Bay (USA). *Estuar. Coast. Shelf Sci.* **57**, 757–781 (2003).

25. M. E. Mann, J. D. Woodruff, J. P. Donnelly, Z. Zhang, Atlantic hurricanes and climate over the past 1,500 years. *Nature.* **460**, 880–883 (2009).

26. J. A. Hogan *et al.*, A Research Framework to Integrate Cross-Ecosystem Responses to Tropical Cyclones. *Bioscience* (2020), doi:10.1093/biosci/biaa034.

Supplementary Materials:
Materials and Methods
Figs. S1 to S9
Tables S1
References

245

Figure 1. Tall mangroves in southwest Florida experienced the greatest canopy height losses from strong winds but storm surge led to mangrove dieback in poorly-drained areas for mangroves in all height classes. (A) Track of Hurricane Irma across Florida. (B) Modeled storm surge from the Coastal Emergency Risk Assessment. (C) Maximum hourly wind speeds from the GEOS-5 model. (D) Estimated canopy height losses. (E) Loss of fractional vegetation cover (FVC) after Hurricane Irma. (F) Estimated recovery time for mangrove forests to pre-storm canopy cover. (G) Photo collected January 2018 in lower Harney River Estuary (H) Photo collected January 2018 in lower Shark River Estuary (I) Photo collected December 2018 in Flamingo. Photo locations are shown in (D).
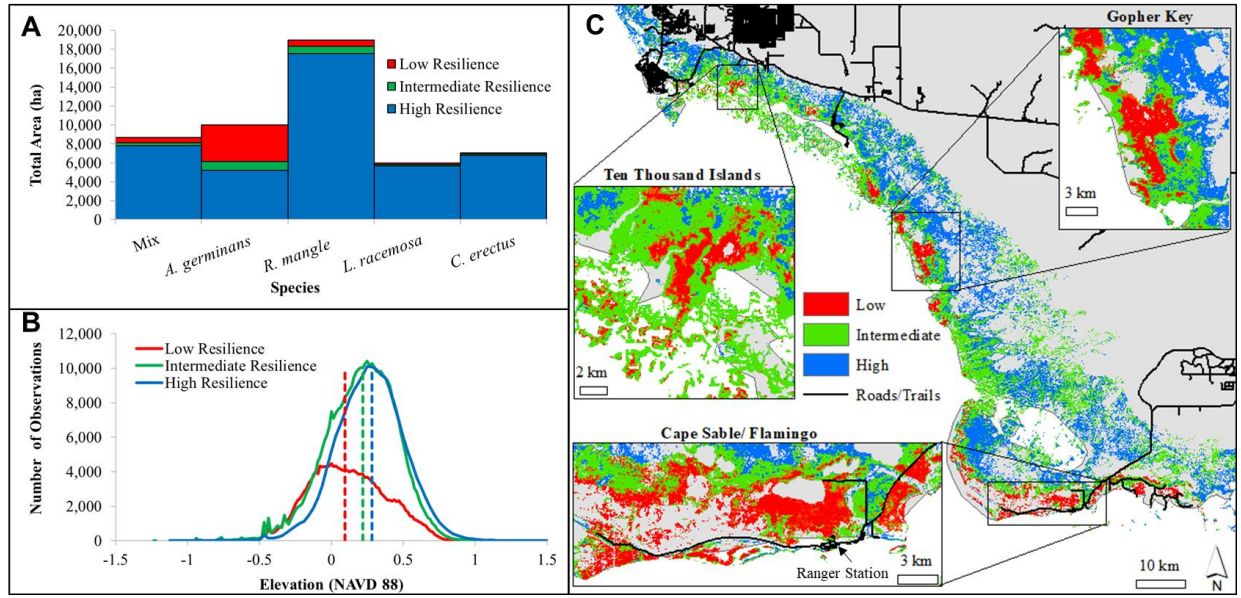
250

255

Figure 2. Mangrove forest dieback was concentrated in low-lying areas dominated by A. germinans, the most salt-tolerant species. (A) Resilience class by species. (B) Distribution of ground elevation for each resilience type. Dashed lines indicate the median elevation values per class. (C) Modeled mangrove resilience across southwest Florida. Hotspots of dieback are highlighted for Ten Thousand Islands, Gopher Key, and Cape Sable/ Flamingo.

260
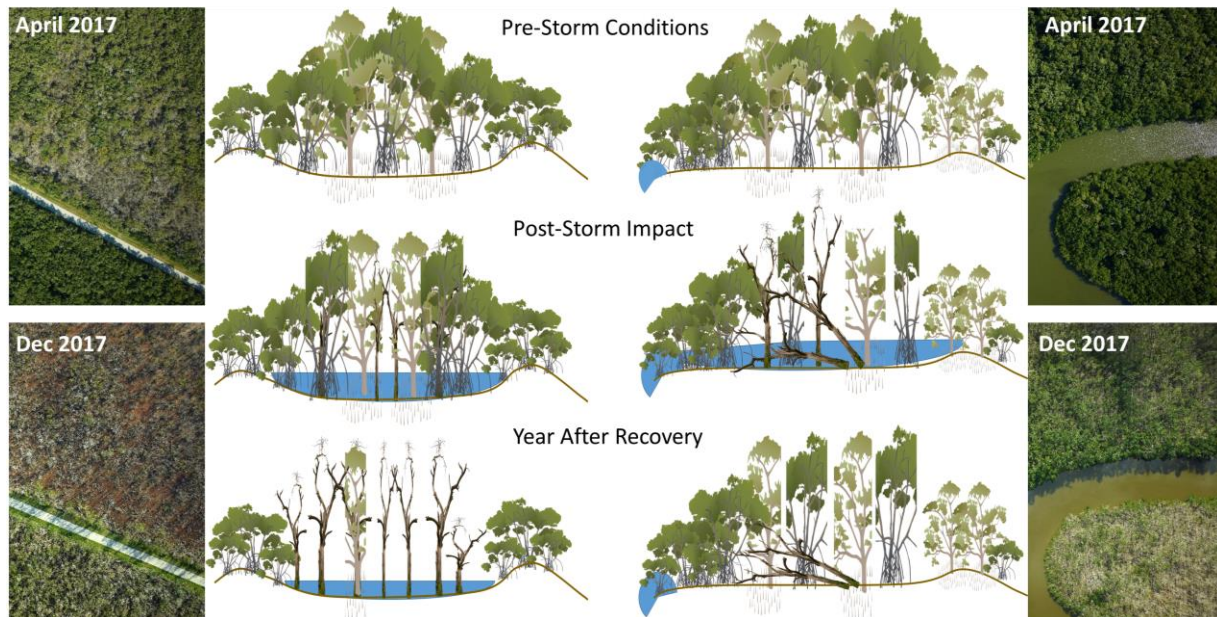
Figure 3. Forest canopy structure, topographic position, and drainage contribute to differences in mangrove vulnerability and resilience to hurricane damages. (A) Areas that flood from saltwater storm surge but do not drain have low resilience, with greatest risk for dieback from hypersalinization and porewater sulfide build up. (B) Mangroves in well-drained (i.e., tidally dominated) sites have high resilience to storm damages and can flush new leaves or resprout quickly after canopy damage from hurricane winds. Aerial photos from NASA's G-LiHT Airborne Imager show examples of mangroves with low and high-resilience in southwest Florida before and after Hurricane Irma.

Table 1. Changes in mean canopy height from Hurricane Irma were greatest in taller mangrove forests. Wind speed classes reflect the maximum one-hour wind speed exposure from Hurricane Irma (17). Colors indicate the mangrove area covered by each height and wind class.

| Canopy Height (m) | Maximum Wind Speed (m sec^{-1}) | | | | | | |
	25-30	30-35	35-40	40-45	45-50	>50	Average
>20 m	-1.36	-1.60	-2.83	-2.91	-3.30	-3.96	-2.97
15-20 m	-3.07	-2.10	-2.18	-2.41	-2.57	-2.72	-2.49
10-15	-2.37	-1.98	-1.72	-2.30	-2.01	-1.10	-2.05
5-10	-1.73	-1.65	-0.95	-1.48	-1.10	-0.73	-1.18
0-5	-0.75	-0.50	-0.28	-0.42	-0.47	-0.54	-0.41
Average	-1.55	-1.41	-0.58	-1.41	-1.25	-0.63	-1.16

Legend:
- Modeled
- <40 ha & SE > 0.1 m
- 60-800 ha
- 801-1500 ha
- 1501-2500 ha
- >2501 ha

280

Materials and Methods

A combination of airborne and satellite remote sensing data were used to quantify changes in mangrove forest structure and function from Hurricane Irma (Fig. S1). Findings based on multi-sensor airborne data were scaled to the entire study area using estimates of forest structure and vegetation phenology derived from satellite data.

G-LiHT Airborne Campaign

During April 2017, NASA Goddard's Lidar, Hyperspectral, and Thermal (G-LiHT) airborne imager conducted an extensive airborne campaign in South Florida covering >130,000 ha. The same flight lines were resurveyed with G-LiHT eight months later, during November and December of 2017, to quantify structural changes in coastal forests of South Florida and Everglades National Park (ENP) following Hurricane Irma (Fig. S2). The analysis of pre and post-hurricane conditions used 1-m resolution lidar data products (Fig. S3) and 3-cm resolution stereo aerial and ground photos (Fig. S4 & S5) to estimate changes in vegetation structure, fractional cover, and terrain heights across the study domain. G-LiHT lidar canopy height models, digital terrain models, and estimates of fractional vegetation canopy cover (FVC) were produced using standard processing methodology (*1*). All Level 1 through 3 lidar data products and fine-resolution imagery are openly shared through the G-LiHT webpage (https://gliht.gsfc.nasa.gov/).

High Resolution Stereo Maps of Canopy Height

Stereo imagery from high-resolution commercial satellites can be used to estimate canopy and terrain surfaces (*2*, *3*). Here, we derived digital surface models (DSMs) from DigitalGlobe's Worldview 2 Level 1B imagery. DigitalGlobe provides these data to U.S. Government agencies and non-profit organizations that support U.S. interests via the NextView license agreement (*4*). The spatial resolution of these data depends on the degree of off-nadir pointing for each acquisition. In this study, image resolution ranged from 0.5 – 0.7 m. We selected along-track stereopairs within the study domain to identify stereo image "strips" (each ~17 km × 110 km) that were nominally cloud-free over the forested domain of interest for years 2012 - 2013, the most recent cloud-free stereo data available for the study region prior to Hurricane Irma. The DSMs were produced using the Ames Stereo Pipeline (ASP) v. 2.5.1 on the NASA Center for Climate Simulation's Advanced Data Analytics Platform at Goddard Space Flight Center (ADAPT, https://www.nccs.nasa.gov/services/adapt). The Worldview DSMs have been shown to accurately estimate mangrove canopy height when compared to airborne lidar and radar interferometry (*2*, *3*). The processing workflow was adapted from (*5*), using algorithms and parameters from (*6*). The ASP processing yielded five DSMs at 1-m resolution that were used to capture pre-storm canopy surface elevations.

Each of the five Worldview DSMs were individually calibrated using overlapping pre-storm G-LiHT lidar data to estimate mangrove canopy heights across the study region (Fig. S1). We sampled 1,000 points within the mangrove forest cover (see mangrove classification, below) to develop a bias-correction equation between G-LiHT lidar-derived canopy heights and stereo DSM elevations (Fig. S6). The bias-corrected canopy height models from high-resolution stereo

imagery were mosaicked together to generate a 1-m resolution CHM for the entire study region (Fig. S7).

Landsat Mangrove Forest Classification

Landsat 8 Operational Land Imager (OLI) imagery was used to map mangrove cover for the southern Florida study region. The imagery was preprocessed to surface reflectance (*7*) and clouds were masked following methods outlined in (*8*). The Surface Reflectance Tier 1 product in Google Earth Engine was used to create a cloud-free image mosaic for 2016 based on the median values of all cloud-free images for the year for all bands (Fig. S1).

Training points were collected using contemporary Google Earth imagery. Twenty four polygons covering a mangrove area of 1243 ha and 17 polygons covering a non-mangrove area of 2759 ha were identified for training regions. Within each of the two classes (i.e., mangrove and non-mangrove), 10000 points were sampled and used for the training data in a Random Forest Classification implemented in Google Earth Engine. The Random Forest model used 20 trees and a bag fraction of 0.5. The Landsat-based mangrove map was validated using the Region 3 species land cover map developed by the National Park Service for Everglades National Park (*9*). The National Park species map was reclassified into mangrove and non-mangrove land cover, and 500 randomly generated points were sampled within each of the two land cover classes. The resulting error matrix indicated an overall accuracy of 90.6%.

Post-Storm Canopy Cover

Time series of Landsat data were used to estimate hurricane damages of mangrove forest cover through December 31, 2017. We combined data from Landsat 7 ETM+ and Landsat 8 OLI to create a dense time series of cloud-free observations. All images were pre-processed to surface reflectance and masked for clouds using the same methods as the mangrove classification. Landsat 7 and Landsat 8 data were then harmonized to account for differences in the sensor specifications following (*10*). We calculated the Normalized Difference Vegetation Index (NDVI) and Normalized Difference Water Index (NDWI) for each image in the collection. We calculated two reference maps from the time series of Landsat imagery (Fig. S1). A pre-storm reference was calculated as the median value for each reflectance and index band for all cloud-free imagery in the two years prior Hurricane Irma, August 31, 2015 through August 31, 2017. Similarly, a post-storm mosaic image was developed using Landsat data between October 1, 2017 and December 31, 2017.

Pre- and post-storm wall-to-wall Fractional Vegetation Cover (FVC) maps were generated using a combination of lidar-based FVC metrics and Landsat imagery (Fig. S1). First, lidar-based FVC was binned into five classes; 0-20%, 20-40%, 40-60%, 60-80% and 80-100% (SI Fig. 8). We then collected 1000 randomly generated points in each of the five FVC classes, a total of 5000 points, to be used as training data in the Landsat classification. Here, we implemented a Random Forest Classifier using 100 trees and a bag fraction of 0.5. These steps were applied to both the pre-storm and post-storm lidar-derived FVC and Landsat mosaic image metrics. Changes between the pre- and post-storm FVC were then calculated based on the five different FVC

classes (Fig. S8). For example, a pixel with pre-storm FVC of 80-100% and a post-storm FVC of 20-40%, a reduction of three FVC classes, was assigned a drop in FVC of 40-60% (Fig. 1).

Recovery Times and Resilience

We estimated the time to full recovery of pre-storm mangrove green canopy cover using the time series of Landsat NDVI during the first 15-months following Hurricane Irma. The pre-storm mean NDVI layer was used as a reference, as described in the previous section. Next we calculated the NDVI anomaly for each image during the post-storm period, September 17, 2017 through December 31, 2018 (Fig. S1). We then summed the individual anomaly values from each Landsat image and normalized by the total number of valid pixels (i.e., pixels meeting quality control measures) to estimate the average change in NDVI within the 15 months after the storm. We used anomaly values to identify mangrove forests with large decreases in the 15 months after the storm using a threshold of 0.2 for the 15-month NDVI average anomaly (*11*, *12*). These areas suffered large losses of canopy material and limited new growth during the post-storm period. We used the slope in NDVI values for each pixel during 2018 to estimate the time in years to full recovery to pre-storm NDVI values, excluding data from October – December 2017 to remove delayed "browning" of damaged vegetation and spurious NDVI values from surface water features following the storm. Areas with a negative NDVI slope were not assigned a recovery time.

We used a combination of the NDVI slope, estimated time to full NDVI recovery, and the average change in NDVI between the pre and post-storm periods to categorize mangrove forest resilience, the potential for mangroves to rebound to pre-disturbance conditions. The specific criteria for mangrove recovery rates and mangrove damage thresholds were adapted from field and remote sensing studies, respectively (*12–14*). Regions of *high resilience* were identified based on rapid recovery and/or little to no immediate impact from the storm: 1) areas that were observed to recover to pre-disturbance conditions during 2018, 2) areas that were predicted to recover within 5 years regardless of the post-storm drop in NDVI (*13*), and 3) regions with a post-storm change in NDVI < -0.1, despite exposure to tropical storm or hurricane-force winds (Fig. S9). The *intermediate resilience* class was classified as areas with predicted recovery times between 5 and 15 years (*13*) and areas with a negative NDVI slope or an extended recovery time but larger initial post-storm drop in NDVI of 0.1 to 0.2 (*14*) (Fig. S9). Lastly, the *low resilience* class of mangrove areas was defined as forests with predicted recovery times > 15 years or a negative NDVI slope that occurred in regions with the largest (> 0.2) post-storm drop in average NDVI (*14*) (Fig. S9).

Mangrove Species and Elevation

We used species level maps developed by the National Park Service for Everglades National Park (*9*) to characterize the impact of Hurricane Irma on different mangrove species. For that study, dominant species were identified through photo-interpretation of stereoscopic, color-infrared aerial imagery. Grid cells of 50 m x 50 m covering an area (Region 3) of ~100,000 ha in southwest Florida were interpreted based on the majority cover type and validated using field observations. A total of 169 vegetation cover classes were identified in this region, however, only five mangrove cover classes were considered for these analyses: *Avicennia germinans*

4

(Black Mangrove), *Laguncularia racemosa* (White Mangrove), *Rhizophora mangle* (Red Mangrove), *Conocarpus erectus* (Buttonwood), and a single mixed species mangrove class. The mangrove species data were reprojected to match the Landsat resolution and the resilience maps. We used the intersection of the resilience and species extent maps to estimate the proportion of each resilience class by dominant species.

The USGS National Elevation Dataset (NED) was used to estimate the soil elevation across southwest Florida. The 1/9 arc second (~3m x 3m) products were acquired from NED, and reprojected to Landsat resolution to estimate the proportion of each resilience class by soil elevation.

Storm Surge, Maximum Hurricane Wind Speed, and Canopy Damage

Modeled maximum storm surge data for Hurricane Irma were acquired from Coastal Emergency Risks Assessment data portal. Storm surge is derived from the ADCIRC Prediction System that solves for time dependent, circulation, and transport in multiple dimensions (*15*).

Maximum sustained hurricane wind speed was modeled hourly at a 5 km x 5 km resolution for 2017 by NASA's Global Modeling and Assimilation Office (GMAO) (*16*). The storm maximum wind speed for each 5 km x 5 km grid cell was calculated and binned into six discrete classes of wind speeds at 5 m sec^{-1} increments: 26-30, 31-35, 36-40, 41-45, 46-50, and >50.

References
1. B. D. Cook *et al.*, NASA Goddard's LiDAR, Hyperspectral and Thermal (G-LiHT) Airborne Imager. *Remote Sens.* **5**, 4045–4066 (2013).
2. D. Lagomasino *et al.*, A Comparison of Mangrove Canopy Height Using Multiple Independent Measurements from Land, Air, and Space. *Remote Sens.* **8**, 327 (2016).
3. D. Lagomasino, T. Fatoyinbo, S. Lee, M. Simard, High-resolution forest canopy height estimation in an African blue carbon ecosystem. *Remote Sens. Ecol. Conserv.* (2015).
4. C. S. R. Neigh, J. G. Masek, J. E. Nickeson, High-resolution satellite data open for government research. *Eos (Washington. DC).* **94**, 121–123 (2013).
5. D. E. Shean *et al.*, An automated, open-source pipeline for mass production of digital elevation models (DEMs) from very-high-resolution commercial stereo satellite imagery. *ISPRS J. Photogramm. Remote Sens.* **116**, 101–117 (2016).
6. P. M. Montesano *et al.*, The use of sun elevation angle for stereogrammetric boreal forest height in open canopies. *Remote Sens. Environ.* **196**, 76–88 (2017).
7. E. Vermote, C. Justice, M. Claverie, B. Franch, Preliminary analysis of the performance of the Landsat 8/OLI land surface reflectance product. *Remote Sens. Environ.* **185**, 46–56 (2016).
8. S. Foga *et al.*, Cloud detection algorithm comparison and validation for operational Landsat data products. *Remote Sens. Environ.* (2017), doi:10.1016/j.rse.2017.03.026.
9. P. L. Ruiz *et al.*, "The Everglades National Park and Big Cypress National Preserve Vegetation Mapping Project: Interim report—Southwest Coastal Everglades (Region 3)" (Fort Collins, Colorado, 2018), , doi:10.13140/RG.2.2.36087.88484.
10. D. P. Roy *et al.*, Characterization of Landsat-7 to Landsat-8 reflective wavelength and

normalized difference vegetation index continuity. *Remote Sens. Environ.* **185**, 57–70 (2016).

11.   D. Lagomasino *et al.*, Measuring mangrove carbon loss and gain in deltas. *Environ. Res. Lett.* **14**, 025002 (2019).

12.   C. Zhang, S. D. Durgan, D. Lagomasino, Modeling risk of mangroves to tropical cyclones: A case study of Hurricane Irma. *Estuar. Coast. Shelf Sci.* **224**, 108–116 (2019).

13.   T. M. Danielson *et al.*, Assessment of Everglades mangrove forest resilience: Implications for above-ground net primary productivity and carbon dynamics. *For. Ecol. Manage.* **404**, 115–125 (2017).

14.   P. Taillie *et al.*, Widespread mangrove damage resulting from the 2017 Atlantic Mega Hurricane Season. *Environ. Res. Lett.* (2020), doi:10.1088/1748-9326/ab82cf.

15.   R. Luettich, J. Westerink, "Formulation and Numerical Implementation of the 2D/3D ADCIRC Finite Element Model Version 44.XX" (2004).

16.   A. Molod, L. Takacs, M. Suarez, J. Bacmeister, Development of the GEOS-5 atmospheric general circulation model: evolution from MERRA to MERRA2. *Geosci. Model Dev*. **8**, 1339–1356 (2015).
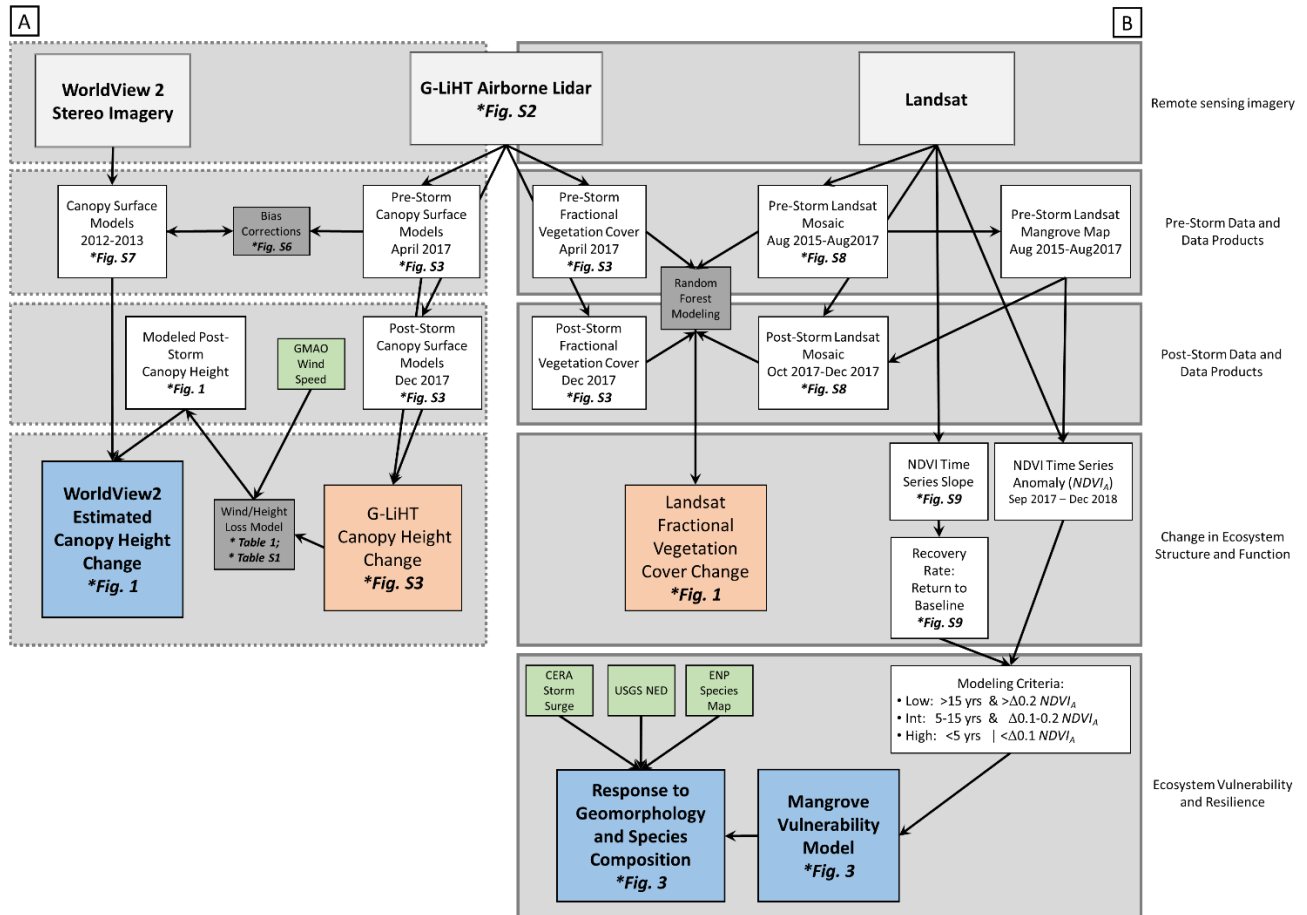
Fig. S1.

This study combined airborne and satellite remote sensing data to quantify changes in mangrove forest structure (A) and function (B) from Hurricane Irma across southwest Florida. Pre-storm wall-to-wall estimates of forest structure from stereo data were calibrated using G-LiHT lidar collected in April 2017. Post-storm canopy height was estimated using a combination of wind speed and G-LiHT lidar canopy height changes. Similarly, lidar data were used to train a model of FVC from Landsat data in order to quantify post-storm changes in canopy cover. Finally, time series of Landsat data were used to track the flushing of new leaves and canopy closure in the 15 months following the storm. The combined information from post-storm estimates of mangrove damage and the time scale for recovery were used to classify mangrove forest resilience. Green boxes represent supplemental dataset not directly derived by this study. Dark grey shaded boxes represent models that combine G-LiHT lidar with satellite or other spatial datasets. White boxes represent intermediate processing steps for dataset generation. Orange boxes indicate disturbance maps. Blue boxes represent the primary data outputs and disturbance maps derived in this study. Asterisks denote the use of derived data products in main text and supplemental figures.
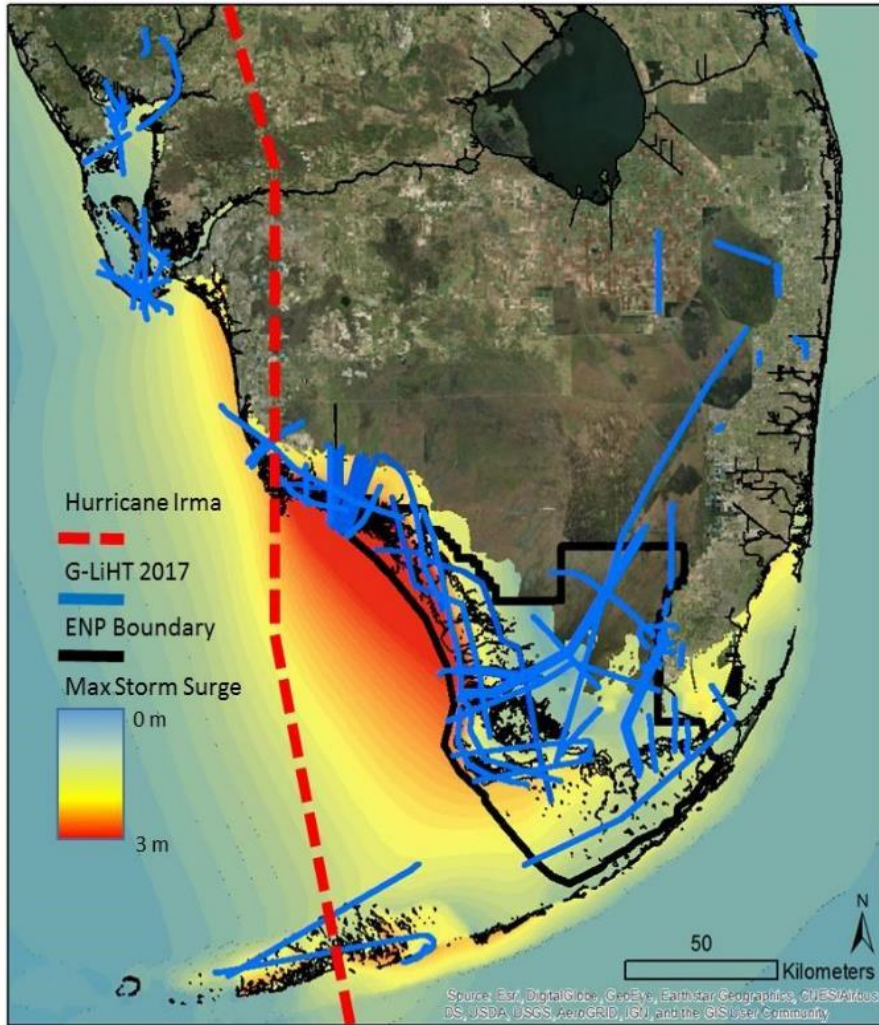
Fig. S2. NASA's G-LiHT Airborne Imager captured pre and post-storm conditions across the study region in southwest Florida. In total, G-LiHT multi-sensor data covered ~130,000 ha over the Florida Keys, Everglades National Park (black outline), and mangrove forests near Port Charlotte, FL. The storm track of Hurricane Irma and modeled storm surge are shown in red.
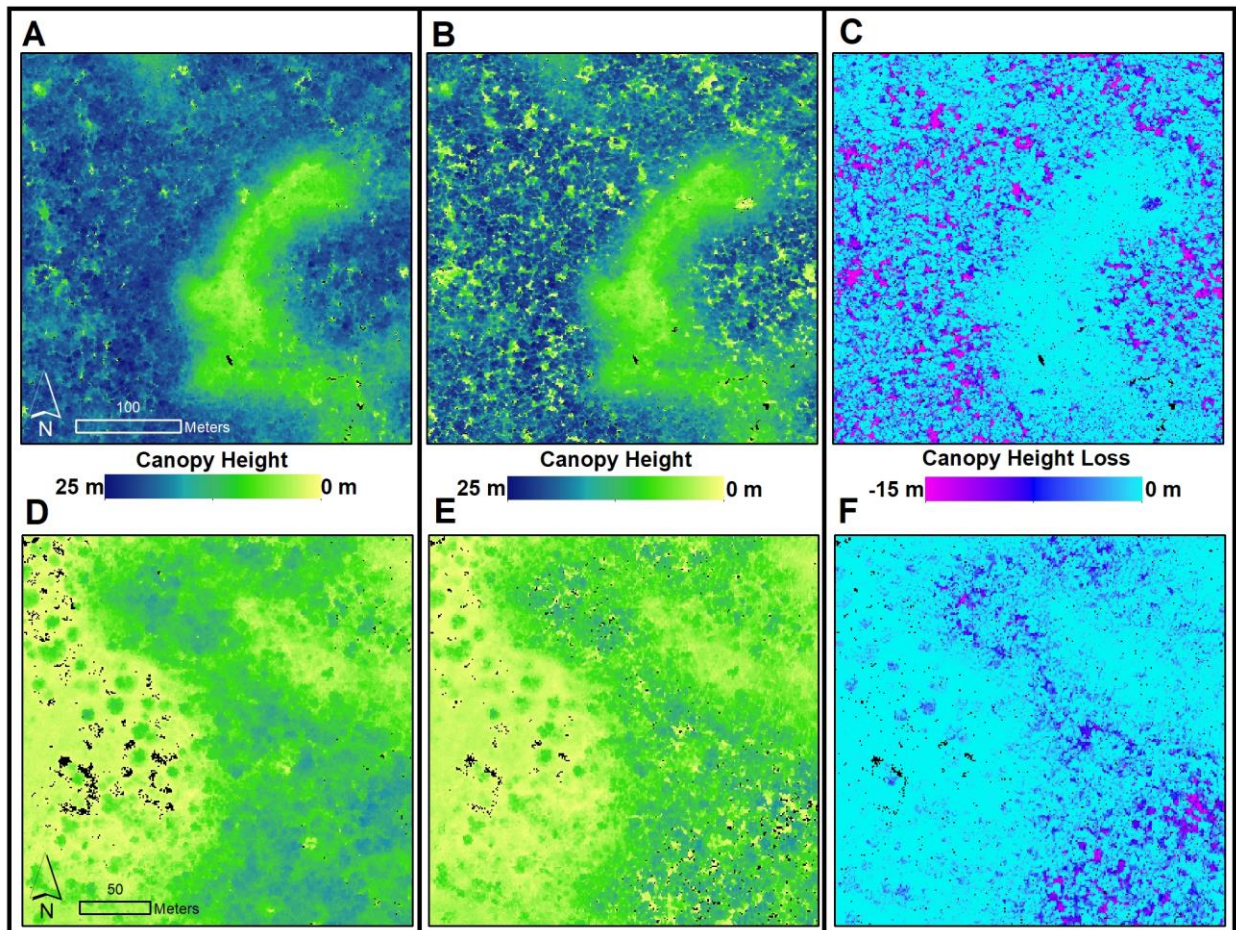
Fig. S3. Repeat airborne lidar data captured fine-scale patterns of mangrove forest damage from Hurricane Irma, with greater height losses in taller forests. Lidar-derived canopy height models for a tall mangrove forest in the Shark River Estuary in April 2017 (A), December 2017 (B), and estimated canopy height losses (C). Lidar-derived canopy height models for a shorter-statured mangrove forest in the lagoon region of Ten Thousand Islands in April 2017 (D), December 2017 (E), and estimated canopy height loss (F). See Figure S4 for high-resolution aerial photos of these forested areas.
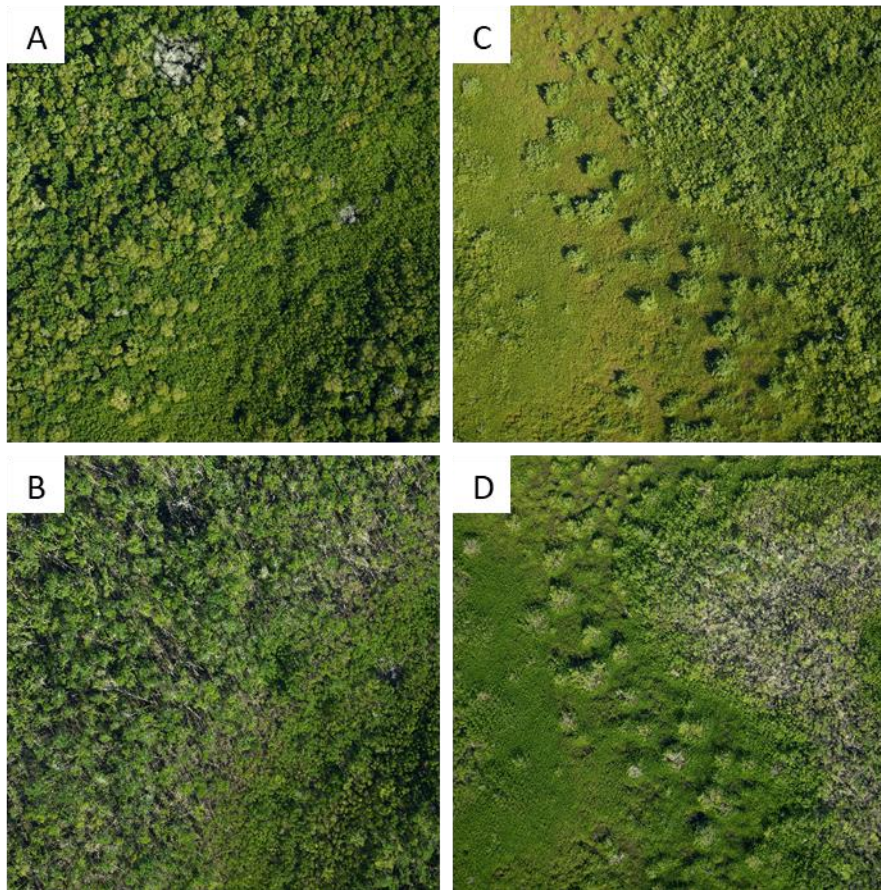
Fig. S4. High-resolution airborne photos from G-LiHT capture details of hurricane impacts on mangrove forests and surrounding herbaceous cover types. Photos (A) and (B) match the pre and post-storm lidar data shown for the Shark River Estuary site shown in Fig. S3 (panels A & B). Similarly, photos (C) and (D) match the pre and post-storm lidar data shown for the Ten Thousand Islands site in Figure S3 (panels D & E).
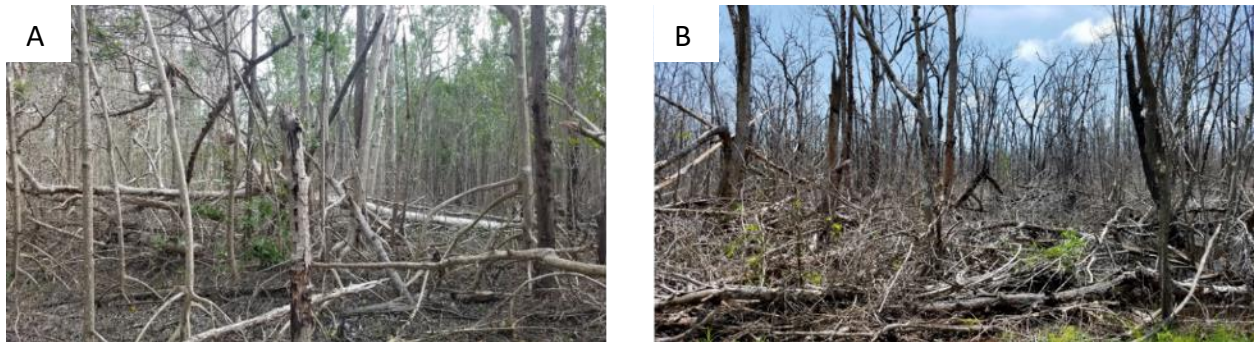
Fig. S5. Field photos confirm the extent of initial mangrove damages and divergent trajectories of forest recovery following Hurricane Irma. Field surveys in January and December of 2018. (A) Field photo collected in January 2018 at a tall (>15 m) mangrove forest site with high resilience. (B) Field photo collected in December 2018 at a mangrove forest with trees 6-12 m and low resilience.
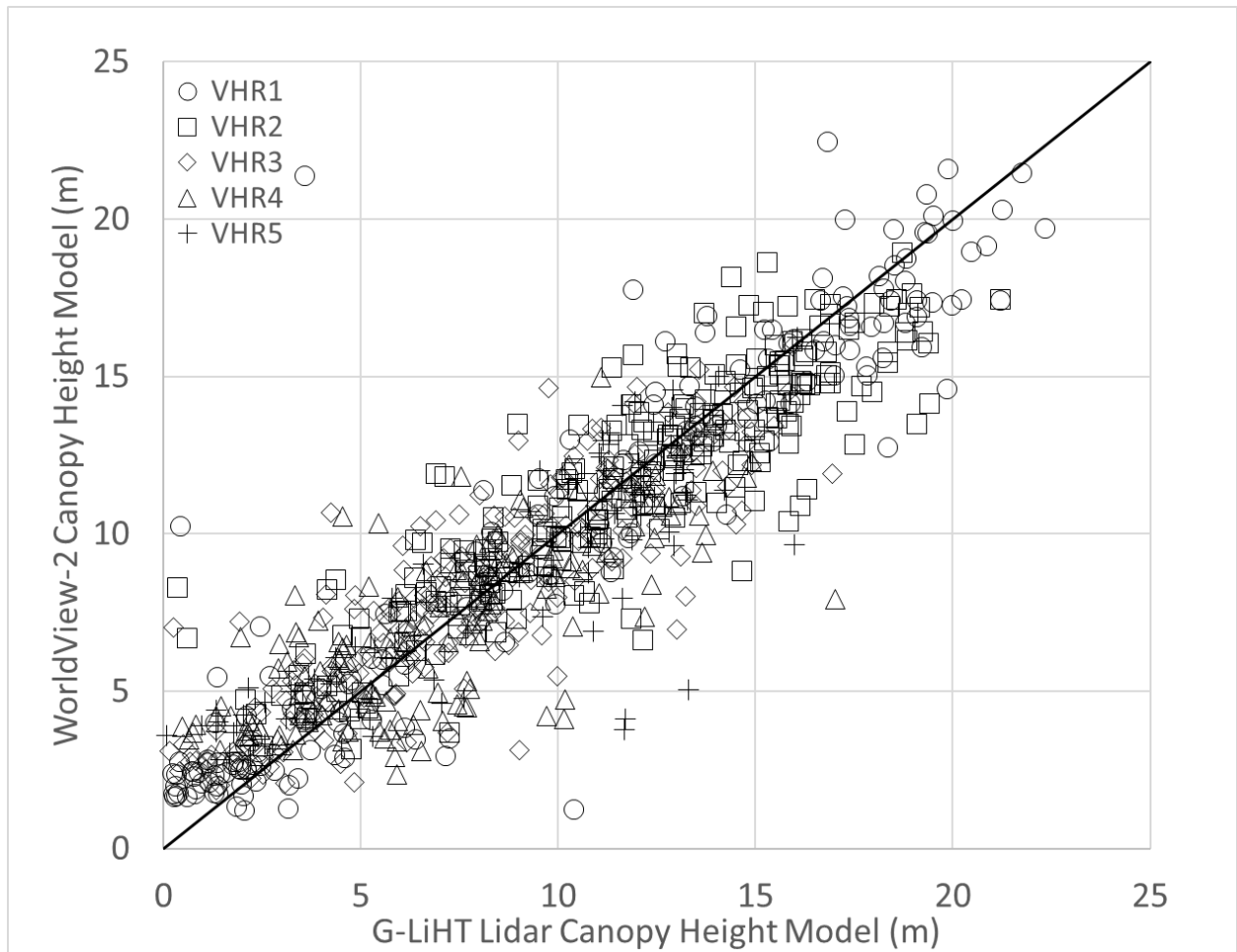
Fig. S6. G-LIHT lidar data were used to correct canopy surface models from very high-resolution (VHR) WorldView 2 stereo satellite imagery to estimate mangrove canopy heights across the study domain. Each VHR image was independently bias-corrected, and the total estimated root mean square error (RMSE) between lidar and WorldView canopy height estimates was 2.2 m. The extent of each VHR image swath is shown in Fig. S7.
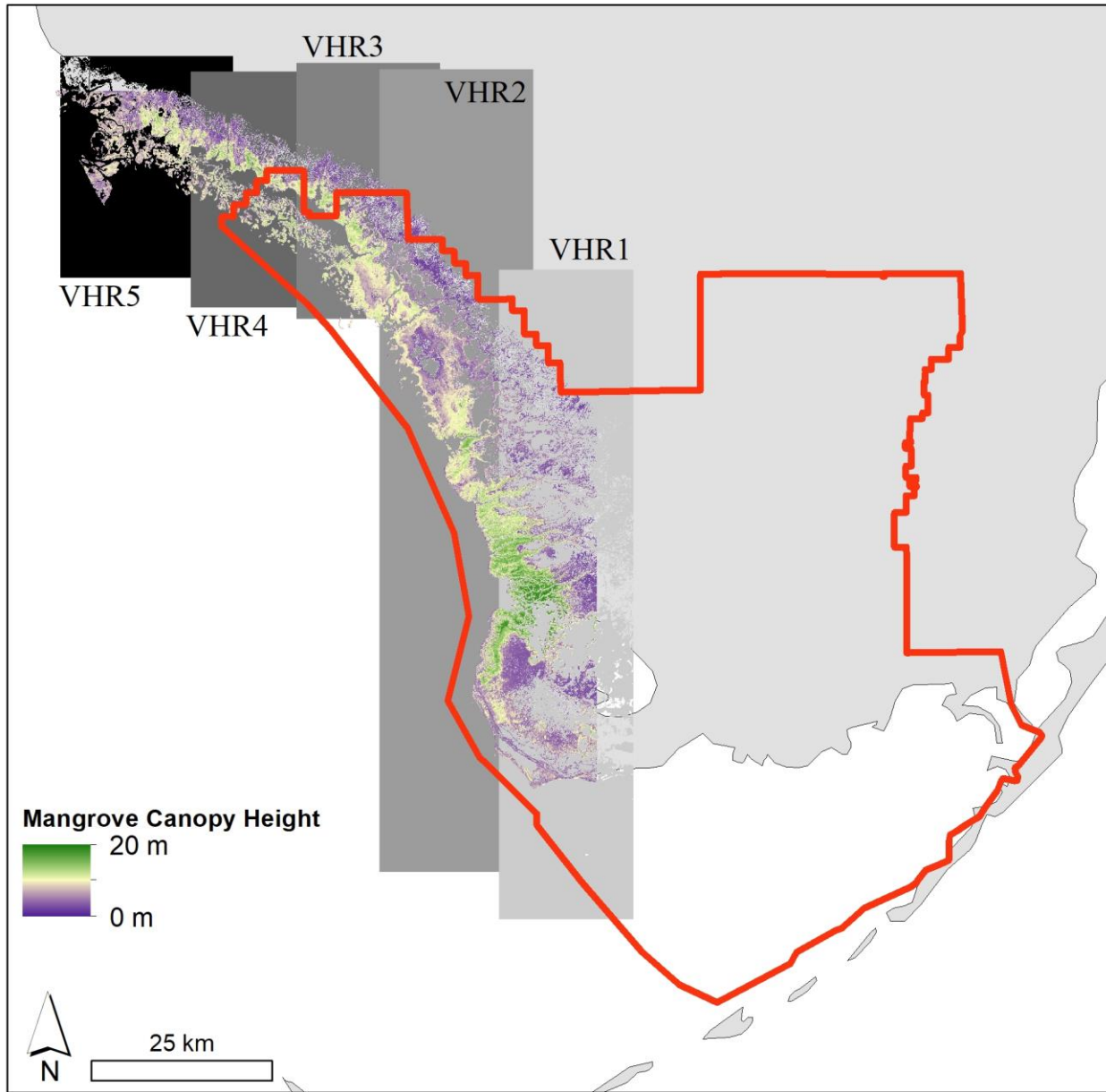
Fig. S7. Five Worldview Digital Surface Models were used to estimate mangrove canopy heights across the study domain in southwest Florida. The boundary of Everglades National Park is shown in red.
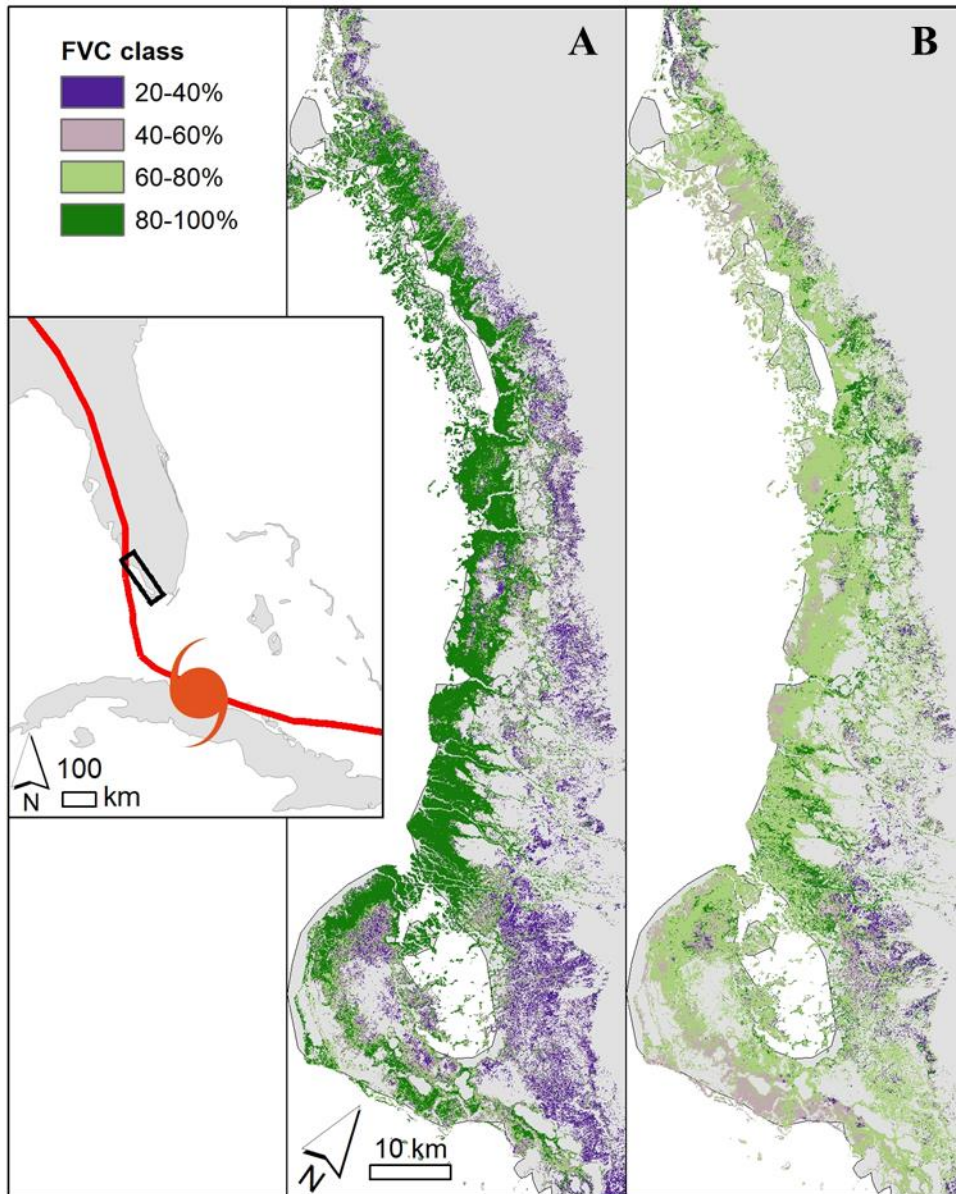
Fig. S8. Mangrove fractional vegetation cover (FVC) before (A) and after (B) Hurricane Irma. For each time period, FVC was calculated from Landsat imagery calibrated using G-LiHT airborne lidar data.
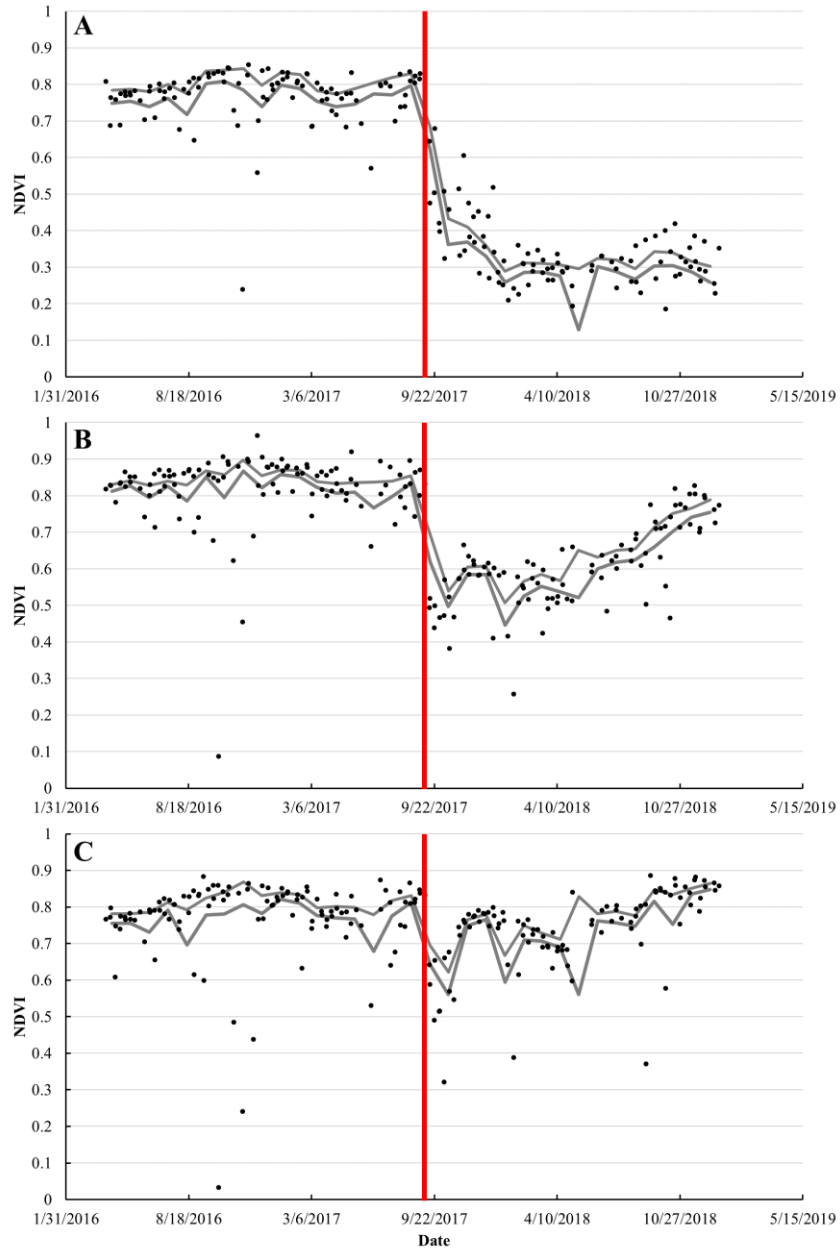
Fig. S9. Normalized Difference Vegetation Index (NDVI) time series for mangrove forests categorized as low resilience (A), intermediate resilience (B), and high resilience (C). Low resilience was marked by a significant and persistent drop in NDVI after the storm with little to no indication of recovery. Conversely, the intermediate and high resilience exhibited disturbance with signs of recovery in the 15-month period after Hurricane Irma. The black dots represent the average of 50 randomly sampled points within each resilience class. The grey lines denote the monthly 95% confidence interval boundaries. The red lines mark the date Hurricane Irma struck South Florida, September 10, 2017.

A.

Canopy Height Classes (meters)	Maximum Wind Classes (kph)					
	25-30	30-35	35-40	40-45	45-50	>50
>20		**0.418**	**0.305**	0.048	**0.103**	
15-20	**0.394**	**0.137**	0.076	0.021	0.015	
10-15	**0.116**	0.049	0.033	0.019	0.009	0.074
5-10	0.057	0.034	0.013	0.010	0.006	0.019
0-5	0.030	0.015	0.003	0.004	0.003	0.014

B.

Canopy Height Classes (meters)	Maximum Wind Classes (kph)						
	25-30	30-35	35-40	40-45	45-50	>50	Total
>20	0.00	0.54	8.73	103.41	23.58	0.00	136.26
15-20	4.14	32.31	88.74	530.28	1043.64	0.00	1699.11
10-15	38.79	99.27	242.91	760.32	2470.32	3.60	3615.21
5-10	67.77	123.84	604.80	1192.95	3057.30	122.94	5169.60
0-5	62.19	120.33	2255.85	1477.89	3702.60	168.39	7787.25
Total	172.89	376.29	3201.03	4064.85	10297.44	1294.93	18407.43

Table S1. Standard errors (A) of estimated height losses from Hurricane Irma were highest for combinations of pre-storm canopy height and maximum sustained wind speed with smaller areal coverage (B). Prior to Hurricane Irma, the majority of mangrove forests in south Florida were ≤ 10 m. Therefore, while taller forests were more vulnerable to damage from hurricane-force winds, the majority of the region experienced intermediate impacts to canopy height and fractional vegetation cover. Bold values in (A) indicate regions with < 50 ha of G-LiHT data coverage across the study region.